Received: 23 September 2022 | Revised: 14 March 2023 | Accepted: 23 March 2023

DOI: 10.1097/HEP.0000000000000427

ORIGINAL ARTICLE

OPEN

Intratumoral microbial heterogeneity affected tumor immune microenvironment and determined clinical outcome of HBV-related HCC

Shengnan Li[1,2] | Han Xia[3] | Zeyu Wang[1] | Xiehua Zhang[1] | Tianqiang Song[1] | Jia Li[2] | Liang Xu[2] | Ningning Zhang[1] | Shu Fan[4] | Qian Li[2] | Qiaoling Zhang[5] | Yingnan Ye[5] | Jiayu Lv[1] | Xiaofen Yue[1] | Hongcheng Lv[1] | Jinpu Yu[5] | Wei Lu[1]

[1]Department of Hepatobiliary Oncology, Liver Cancer Center, Tianjin Medical University Cancer Institute and Hospital, National Clinical Research Center for Cancer, Key Laboratory of Cancer Prevention and Therapy, Tianjin's Clinical Research Center for Cancer, Tianjin Medical University, Tianjin, China

[2]Department of Hepatology, Tianjin Second People's Hospital, Tianjin Institute of Hepatology, Tianjin, China

[3]School of Automation Science and Engineering, Xi'an Jiaotong University, Xian, China

[4]Department of Scientific Affairs, Hugobiotech Co., Ltd., Beijing, China

[5]Cancer Molecular Diagnostics Core, Tianjin Medical University Cancer Institute and Hospital, National Clinical Research Center of Caner, Key Laboratory of Cancer Prevention and Therapy, Key Laboratory of Cancer Immunology and Biotherapy, Tianjin's Clinical Research Center for Cancer, Tianjin Medical University, Tianjin, China

Correspondence
Wei Lu, Department of Hepatobiliary Oncology, Tianjin Medical University Cancer Institute and Hospital, National Clinical Research Center for Cancer, Key Laboratory of Cancer Prevention and Therapy, Tianjin's Clinical Research Center for Cancer, Tianjin, 300060, China.
Email: luwei1966@126.com

Jinpu Yu, Cancer Molecular Diagnostics Core, Tianjin Medical University Cancer Institute and Hospital, National Clinical Research Center of Caner, Key Laboratory of Cancer Prevention and Therapy, Key Laboratory of Cancer Immunology and Biotherapy, Tianjin's Clinical Research Center for Cancer, Tianjin Medical University, Tianjin, 300060, China.
Email: jyu@tmu.edu.cn

Abstract

Background and Aims: The intratumoral microbiome has been reported to regulate the development and progression of cancers. We aimed to characterize intratumoral microbial heterogeneity (IMH) and establish microbiome-based molecular subtyping of HBV-related HCC to elucidate the correlation between IMH and HCC tumorigenesis.

Approach and Results: A case-control study was designed to investigate microbial landscape and characteristic microbial signatures of HBV-related HCC tissues adopting metagenomics next-generation sequencing. Microbiome-based molecular subtyping of HCC tissues was established by nonmetric multidimensional scaling. The tumor immune microenvironment of 2 molecular subtypes was characterized by EPIC and CIBERSORT based on RNA-seq and verified by immunohistochemistry. The gene set variation analysis was adopted to explore the crosstalk between the immune and

Abbreviations: BP, biological process; CAF, cancer-associated fibroblast; CC, cellular component; CHB, chronic hepatitis B; DEGs, differentially expressed genes; GO, gene ontology; GSVA, gene set variation analysis; IHC, immunohistochemistry; IMH, intratumoral microbial heterogeneity; LDA, linear discriminant analysis; LEfSe, linear discriminant analysis effect size; MF, molecular function; mNGS, metagenomic next-generation sequencing; NMDS, nonmetric multidimensional scaling; PCoA, principal coordinate analysis; TME, tumor microenvironment.

Shengnan Li and Han Xia contributed equally to this article.

Supplemental Digital Content is available for this article. Direct URL citations are provided in the HTML and PDF versions of this article on the journal's website, www.hepjournal.com.

metabolism microenvironment. A prognosis-related gene risk signature between 2 subtypes was constructed by the weighted gene coexpression network analysis and the Cox regression analysis and then verified by the Kaplan-Meier survival curve.

IMH demonstrated in HBV-related HCC tissues was comparably lower than that in chronic hepatitis tissues. Two microbiome-based HCC molecular subtypes, defined as bacteria- and virus-dominant subtypes, were established and significantly correlated with discrepant clinical-pathologic features. Higher infiltration of M2 macrophage was detected in the bacteria-dominant subtype with to the virus-dominant subtype, accompanied by multiple upregulated metabolism pathways. Furthermore, a 3-gene risk signature containing *CSAG4*, *PIP4P2*, and *TOMM5* was filtered out, which could predict the clinical prognosis of HCC patients accurately using the Cancer Genome Atlas data.

Conclusions: Microbiome-based molecular subtyping demonstrated IMH of HBV-related HCC was correlated with a disparity in clinical-pathologic features and tumor microenvironment (TME), which might be proposed as a biomarker for prognosis prediction of HCC.

INTRODUCTION

HCC is an aggressive malignancy with poor prognosis and high recurrence, which commonly occurs on the basis of chronic hepatitis *B* (CHB) in Asia-Pacific.[1–3] The clinical outcomes and treatment efficacies vary significantly even for patients at the same clinical stage due to its high heterogeneity.[3,4] Based on this, a variety of molecular subtyping of HCC has been established, which provides a basis for developing effective targeted therapies and evaluating the prognosis.

It is well known that genetic and epigenetic changes in tumor cells contribute to tumor malignant potential significantly. Transcriptome classification of HCC indicates tumor heterogeneity from pathogenesis and biological behavior.[5–8] A meta-analysis of gene expression profiles in data sets from 8 independent patient cohorts across the world defined 3 HCC subtypes (S1–S3); each correlated with clinical parameters, such as tumor size, tumor differentiation, and serum alpha-fetoprotein levels.[9] In recent years, tumor microenvironment (TME) has been demonstrated to play important roles in tumorigenesis and prognosis,[10,11] and a series of molecular subtyping of HCC has been established based on TME. For example, Sia et al[12] identified an immune-specific classification of HCC based on immune-related molecular features, characterized by adaptive or exhausted immune responses, which might be susceptible to therapeutic agents designed to block the regulatory pathways in T cells, such as programmed death-ligand 1. Fan et al creatively classified HBV-related HCC into 3 subtypes based on metabolic features, characterized by reprogramming, microenvironment imbalance, cell proliferation, and potential therapy,[13] while more classification is needed to foster precision medicine and pave the way for novel therapeutic strategies.[14,15]

With the development of next-generation sequencing technology, the intratumoral microbiome has been regarded as a component of the TME. It was reported to regulate tumorigenesis, development, and prognosis of gastrointestinal tumors.[11,16] Takuji et al revealed distinct stage-specific phenotypes of intestinal microbiota in colorectal cancer by metagenomic sequencing, revealing that specific biomarkers could help to distinguish colorectal cancer from healthy samples.[17] Meanwhile, the tumor microbiome was indicated to contribute to an aggressive phenotype in the basal-like subtype by characterizing the intratumoral microbiome of different pancreatic adenocarcinoma subtypes adopting microbial metagenomic sequencing.[18] This revealed the heterogeneity of pancreatic adenocarcinoma from a microbial perspective. However, as we know, there are very limited studies about molecular subtyping of HBV-related HCC by characterizing intratumoral microbial landscape adopting metagenome sequencing. Therefore, we aimed to establish molecular subtyping based on intratumoral microbial heterogeneity (IMH) of HBV-related HCC tissues, which would provide new insights into tumor heterogeneity and propose a biomarker for prognosis prediction of HCC.

METHODS

Patient enrollment

Two independent cohorts, including 29 HCC cases that underwent partial liver resection operation at the Hepatology Department of TJMUCH and 12 CHB cases that underwent liver puncture biopsy at Tianjin Second People's Hospital from July 2020 to April 2021, were enrolled in this study. All patients were complicated with chronic HBV infection with no history of antibiotics, chemoradiotherapy, or other treatments in the past 3 months. HCC and CHB were diagnosed pathologically by 2 experienced pathologists. Twenty-nine pairs of tumor tissues and corresponding adjacent tissues (>2 cm from the edge of the tumor) were collected from the HCC cohort. 12 cases of liver puncture tissues were collected from the CHB cohort as nontumor controls. A total of 70 samples were collected aseptically and stored at −80 °C within 30 minutes. HCC cohort was followed up every 3 months after operation through outpatient service and telephone consultation, and the median follow-ups were 12 months. HCC recurrence was defined as the development of a new tumor in the remaining liver or distant extrahepatic metastasis. Meanwhile, clinical and pathologic data were collected from an electronic medical history system. The research was conducted in accordance with both the Declarations of Helsinki and Istanbul. This study was approved by the Ethics Committee of Tianjin Medical University (No. E20210132), and informed consent was obtained from all patients.

DNA extraction, library preparation, and sequencing

All snap-frozen tissue samples were sent to Hugobiotech for PACEseq metagenomic next-generation sequencing (mNGS). DNA was extracted from 70 samples with TIANamp Micro DNA Kit (TIANGEN BIOTECH) according to the manufacturer's instructions. Libraries were constructed by TruePrep DNA Library Prep Kit V2 for Illumina TD502 (Vazyme) according to the manufacturer's instructions. To ensure stringent quality control, negative controls—water at the DNA extraction step (NTC-1 and NTC-2) and water at the first PCR step (NTC-3)—were set up during the experiment. The qualities of all libraries were then assessed using Qubit (Thermo Fisher) and Agilent 2100 Bioanalyzer (Agilent). Finally, the qualified libraries were sequenced on an Illumina Next seq. 550 platform (Illumina). After sequencing, short, low-quality, and low-complexity reads were removed from the raw data. Human sequences were also excluded after mapping to the human reference genome (hg38) using the Burrows-Wheeler Aligner. The remaining data were finally aligned to Kraken2 Databases to identify microbial species by k-mer using kraken2 v2.1.1.

RNA extraction, alignment, and gene quantification

Based on the results of DNA mNGS, we screened 24 samples (12 paired tumor tissues and corresponding adjacent tissues) for transcriptome sequencing. RNA was extracted with QIAGEN RNeasy Plus Mini Kit (QIAGEN), and cDNA was then generated using reverse transcriptase and deoxynucleotide triphosphate. Clean reads were obtained from the original data after quality control using fastp (v0.20.0) and then filtered by rRNA from SILVA (v138.1) using bowite2 (v2.2.4). The remaining data were finally aligned to the human genome (GRCh38.101) using hisat2 (v2.2.1). Gene quantification was performed using featureCounts (v2.0.1).

Bioinformatics analysis

Chao 1, Shannon, and Simpson indexes were calculated to analyze microbial alpha diversity. Bray-Curtis distance metrics by the principal coordinate analysis and nonmetric multidimensional scaling were used to analyze microbial beta diversity. The Bray-Curtis distance-based analysis of similarities (Anosim) and the multiresponse permutation procedure were used to evaluate the differences in microbial community structure among groups. Biomarkers with significant differences were identified by the linear discriminant analysis effect size (LEfSe) analysis and the random forest analysis using *R*. The global gene expression profiles were determined, and a threshold of $p < 0.01$ and $|\log_2\text{FoldChange}| \geq 1$ was used to identify differentially expressed genes (DEGs). The "ggplot2" and "pheatmap" packages in *R* were used to plot the heatmap and volcano map of DEGs. The gene ontology enrichment analysis was performed for the functional analysis of DEGs ($p < 0.01$) by the "clusterProfiler" package in *R*. To evaluate the tumor immune microenvironment, EPIC was used to estimate the proportion of immune and tumor cells by calculating a large amount of tumor gene expression data (http://epic.gfellerlab.org/), and CIBERSORT was further performed based on RNA-seq data, of which genes with gene value equaled to 0 and more than 30% were deleted. The gene set variation analysis (GSVA) was performed to calculate the enrichment score of each KEGG metabolic pathway in each sample using the "GSVA" package in *R*.

Immunohistochemistry

A total of 29 samples of paraffin-embedded tumor tissues of HCC were serially cut into 4 μm sections and processed for hematoxylin and eosin and immunohistochemistry staining. Sections were incubated with

monoclonal antibodies against CD3 (ab16669, Abcam), CD8 (ab93278, Abcam), CD68 (ZM-0060, ZSBio), CD163 (ZM-0428, ZSBio), and PD-L1 (ab210931, Abcam) and then stained with avidin-biotin-peroxidase complex method, as described.[19] Negative controls that omitted the primary antibody were included in all assays. Primary antibodies and dilutions were listed in Supplemental Table S1 (http://links.lww.com/HEP/H817). The stained tissue sections were digitally scanned on an Olympus BX51 microscope for image acquisition. Cells stained brownish yellow in the cell membrane or the cytoplasm were regarded as positive. To evaluate CD3, CD8, CD68, and CD163, we counted the numbers of positive cells in 5 fields at 200 magnifications and took the average as the final result. To evaluate PD-L1, stained tissue sections were first observed at 100 magnifications to identify hotspots with the highest density of PD-L1 and then took the average of positive cells in 5 fields at 400 magnification as the final results. All the results were assessed by 2 experienced pathologists separately.

Weighted gene coexpression network analysis analysis and prognosis-related risk signature construction

DEGs between two molecular subtypes of HCC were clustered into highly interconnected gene set modules by the weighted gene coexpression analysis, and the module with the highest correlation with concerned clinical characteristics was screened as a hub module. Hub genes were identified according to an absolute value of module membership >0.7 and gene significance >0.2 by the Pearson correlation analysis. Clinical and RNA-seq data of HCC were obtained from the Cancer Genome Atlas database, and the Cox regression analysis was performed to screen overall survive-related hub genes, so as to construct prognosis-related risk signature. Patients were classified into a high-risk group and a low-risk group by median risk score, and then, the Kaplan-Meier survival curve was used to evaluate the predictive ability of the gene risk signature.

Statistical analysis

Continuous variables were expressed as mean $\pm$ SD, and categorical variables were expressed as absolute and relative frequencies. Differences in continuous variables were analyzed using Student *t* test or the Mann-Whitney *U* test, while the Chi-square test or Fisher exact test was used for categorical variables. The Wilcoxon rank sum test was used to test significant differences between different groups. All statistical tests were 2-sided, and $p < 0.05$ was considered to be statistically significant. Statistical analysis was performed using *SPSS 25.0* software (*SPSS* Inc.). All graphs were drawn by GraphPad Prism software version 9.0.

RESULTS

Intratumoral microbial landscape of HCC was heterogeneous

A total of 70 samples, including 12 CHB tissues and 29 pairs of tumors and corresponding adjacent tissues of HCC, were collected from 41 patients. CHB cohort ($n = 12$) included 8 males and 4 females, ages ranging from 23 to 62 years; the HCC cohort ($n = 29$) included 26 males and 3 females, ages ranging from 30 to 79 years.

Based on mNGS, 13 phyla, 15 classes, 31 orders, 39 families, 58 genera, and 107 species were finally detected. Proteobacteria and artverviricota were the dominant phyla, followed by actinobacteria, peploviricota, uroviricota, apicomplexa, firmicutes, basidiomycota, ascomycota, tenericutes, and so on (Figure 1A). Revtraviricetes, gammaproteobacteria, and alphaproteobacteria were the top 3 microbes at the class level, and blubervirales, enterobacterales, and rhizobiales were dominant at the order level. At the family level, hepadnaviridae, enterobacteriaceae, and methylobacteriaceae were with relatively higher abundances. The dominant compositions of microorganisms at class, order, and family levels were shown in Supplemental Figure S1A, (http://links.lww.com/HEP/H818), S1B, (http://links.lww.com/HEP/H818), and S1C, (http://links.lww.com/HEP/H818), respectively. Orthohepadnavirus, *Escherichia, Shigella, Methylobacterium, Klebsiella, Cutibacterium,* Roseolovirus, *Acinetobacter, Pseudomonas,* and *Ralstonia* were dominant at the genus level. HBV*, Escherichia coli, Shigella dysenteriae, Methylobacterium sp. XJLW, Cutibacterium acnes,* Human betaherpesvirus 6B*, Klebsiella pneumonia, Ralstonia pickettii, Methylobacterium oryzae,* and *Serratia marcescens* were dominant at the species level. The relative abundances of the top 20 microbes at genus and species levels were exhibited in Figures 1B, C. In contrast, almost no microbiota was detected in the negative controls (NTC-1, NTC-2, and NTC-3).

Compared with nontumor tissues, the relative abundances of proteobacteria, firmicutes, and actinobacteria were lower in the tumor tissues at the phylum level, while the relative abundance of artverviricota was higher (Figure 2A). At the class level, the relative abundances of gammaproteobacteria, betaproteobacteria, and actinobacteria were lower in the tumor tissues, while the relative abundance of revtraviticetes was higher (Figure 2B).

To rank the greatest differences in abundant microbes between tumor tissues and nontumor tissues, the LEfSe analysis was conducted. As displayed in Figure 2C, D,

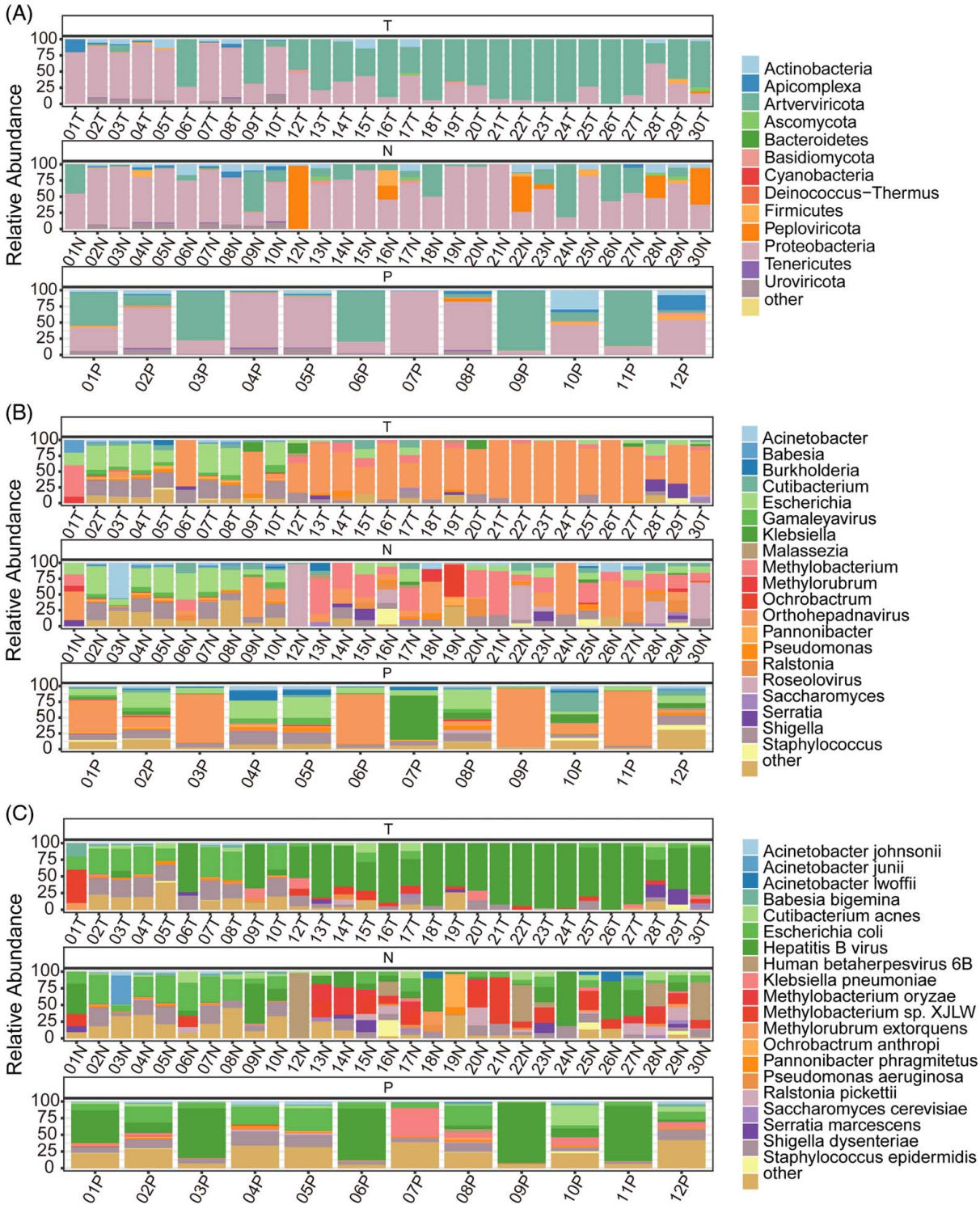

FIGURE 1 Intratumoral microbial landscape of HCC was heterogeneous. Microbial community structure of tumor tissues (T), corresponding adjacent tissues (N), and CHB puncture tissues (P) at the phylum level (A), genus level (B), and species level (C). Bars represent relative abundance. Abbreviation: CHB, chronic hepatitis B.

there was an enrichment of HBV in tumor tissues, while human betaherpesvirus 6B*, Methylobacterium sp XJLW, Ralstonia pickettii,* and *Methylobacterium oryzae* were enriched in the corresponding adjacent tissues according to linear discriminant analysis (LDA) score (threshold value with LDA $>$ 4). Compared with the CHB tissues, *Methylobacterium sp XJLW* was enriched in tumor tissues, while *Klebsiella variicola* were enriched in the CHB tissues.

Furthermore, we analyzed the correlation between these differential microbes with clinicopathological data and found that HBV might be associated with tumor

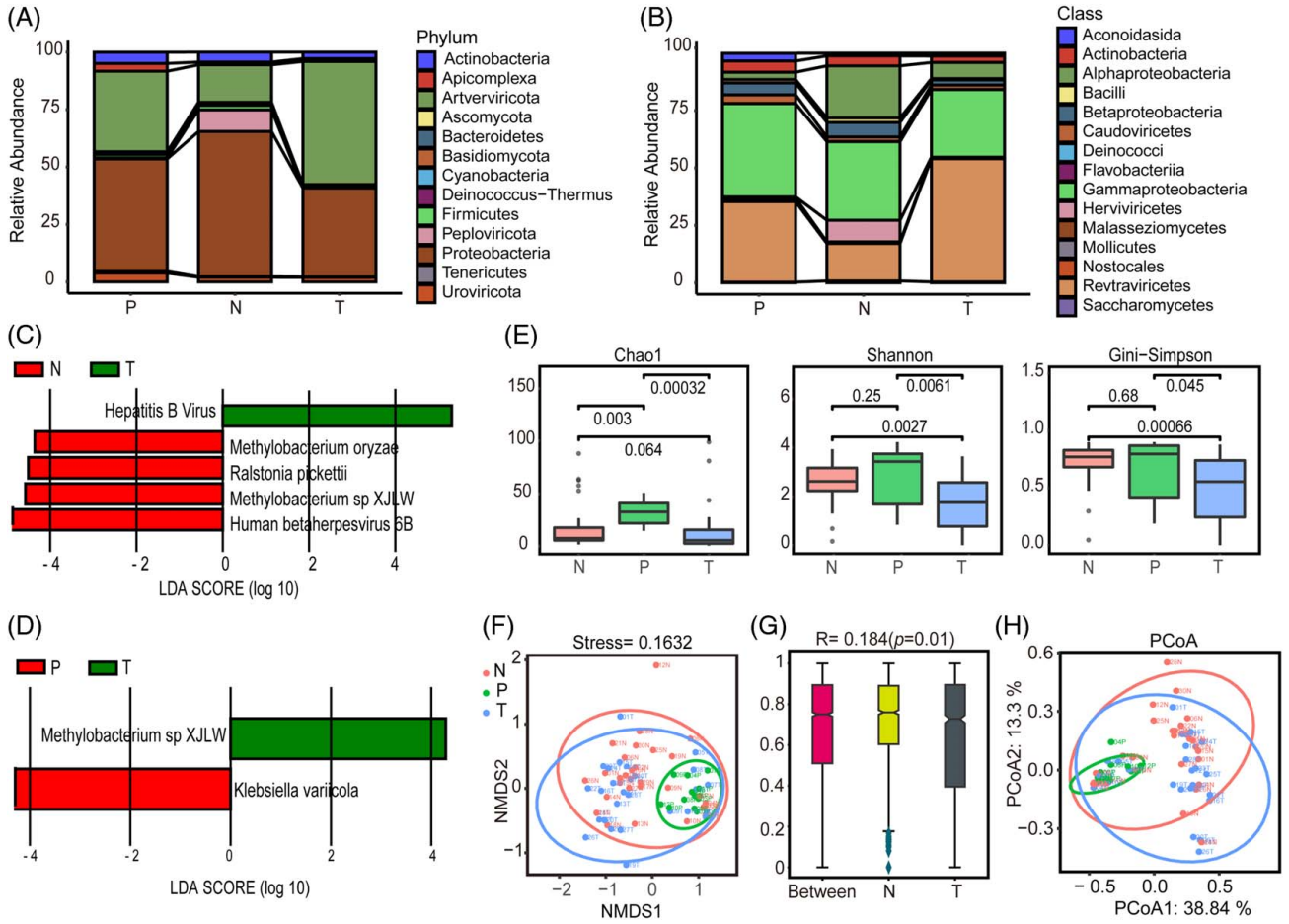

FIGURE 2 IMH of HCC tissues decreased compared with that of nontumor tissues. (A and B) Comparison of microbes with the greatest differences in relative abundance between tumor tissues and nontumor tissues at the phylum level and the class level. (C and D) Microbes with the greatest differences in relative abundance between tumor tissues with corresponding adjacent tissues and CHB tissues by the LEfSe analysis. Threshold value with LDA score >4. (E) Comparison of microbial alpha diversity between tumor tissues and nontumor tissues by Chao 1, Shannon, and Simpson indexes. (F and H) Comparison of microbial structure variability between tumor tissues and nontumor tissues by NMDS and PCoA. (G) Microbial structure differences measured by the Anosim analysis between tumor tissues and corresponding adjacent tissues. Abbreviations: CHB, chronic hepatitis B; IMH, intratumoral microbial heterogeneity; LDA, linear discriminant analysis; LEfSe, linear discriminant analysis effect size; NMDS, nonmetric multidimensional scaling; PCoA, principal coordinate analysis.

differentiation ($p = 0.05$), while no significant correlations were found with other microbes ($p > 0.05$) (Supplemental Table S2, http://links.lww.com/HEP/H819).

Intratumoral microbial heterogeneity of HCC tissues decreased compared with that of nontumor tissues

Analysis of alpha and beta diversity showed that the microbial community structure of tumor tissues was significantly different from that of the corresponding adjacent tissues and CHB tissues. According to the Shannon and Simpson indexes, the richness and evenness of tumor tissues were significantly lower than those of the corresponding adjacent tissues and CHB tissues ($p < 0.01$). The Chao1 index analysis also showed that the alpha diversity of microbes in tumor tissues was significantly lower than that of CHB tissues ($p < 0.05$). In addition, nonmetric multidimensional scaling analysis showed that tumor tissues formed a distinct cluster compared with the nontumor tissues (Figure 2F), and the Anosim analysis indicated significant differences between tumor tissues and the corresponding adjacent tissues ($R = 0.184$ and $p = 0.01$) (Figure 2G). principal coordinate analysis by the Bray-Curtis distance also confirmed the variability in microbial composition among the 3 groups (Figure 2H).

Microbiome-based molecular subtyping of HCC was established on distinct microbial signatures

According to nonmetric multidimensional scaling, the 29 cases of tumor tissues could be classified into 2 molecular subtypes based on microbial signatures (Figure 3A). One subtype was with a microbial community structure

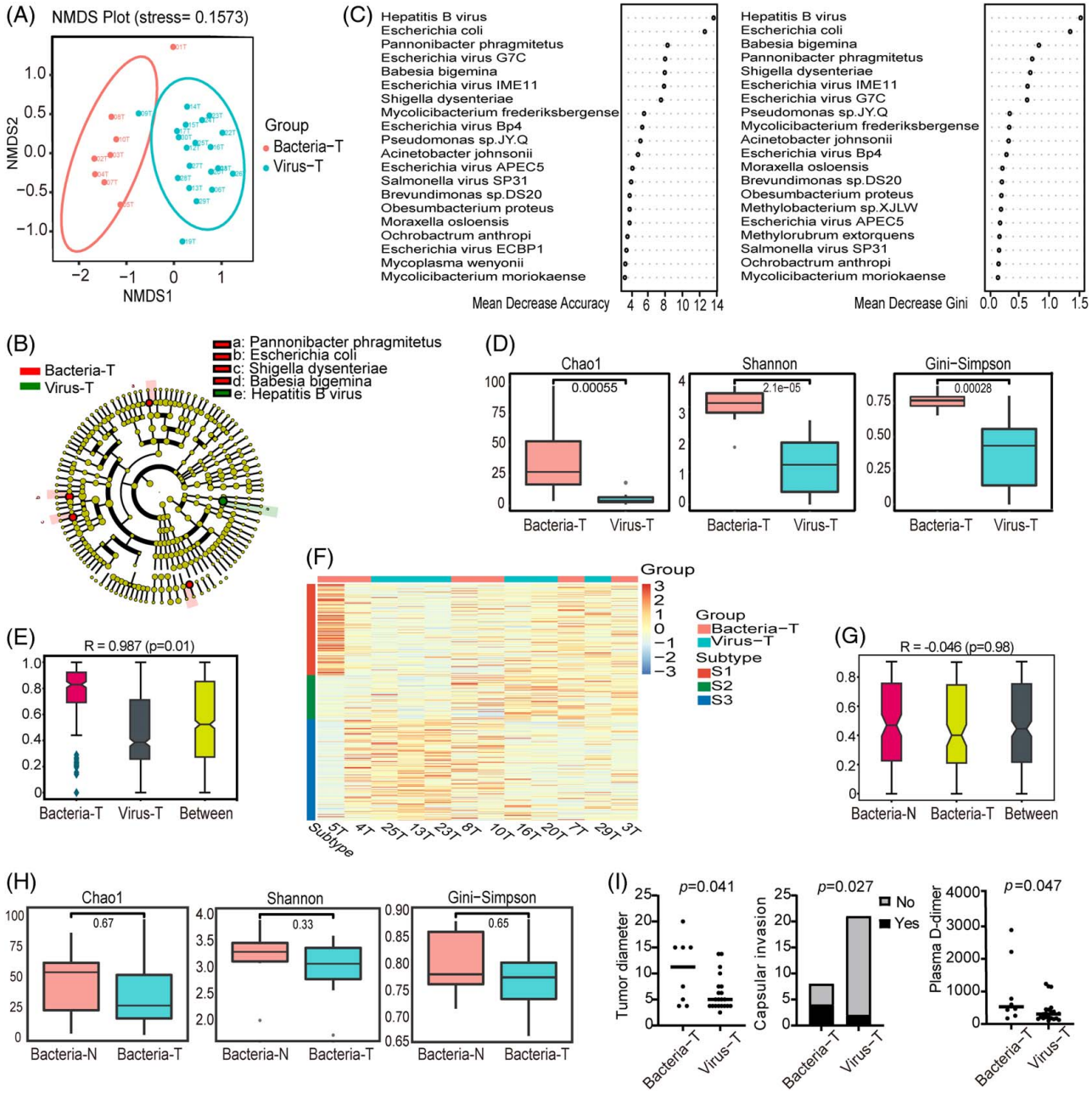

FIGURE 3 Two HCC molecular subtypes were established based on microbial signatures and correlated with discrepant clinical outcomes. (A) Two HCC molecular subtypes were established based on NMDS analysis. (B and C) Species with significant differences in relative abundance between 2 HCC molecular subtypes by LDA effect size taxonomic cladogram (threshold value with LDA score >4) and random forest analysis. (D) Comparison of microbial alpha diversity analysis between two HCC molecular subtypes by Chao 1, Shannon, and Simpson indexes. (E) Microbial structure differences measured by the Anosim analysis between two HCC molecular subtypes. (F) Association between IMH-based molecular subtype with typical molecular subclassification of HCC established on the basis of a large cohort.[9] (G) Microbial structure differences measured by the Anosim analysis between tumor tissues (Bacteria-*T*) and corresponding adjacent tissues (Bacteria-*N*). (H) Comparison of microbial alpha diversity analysis between Bacteria-*T* and Bacteria-*N* by Chao 1, Shannon, and Simpson indexes. (I) Comparison of clinical-pathologic features between two HCC molecular subtypes. Abbreviations: IMH, intratumoral microbial heterogeneity; LDA, linear discriminant analysis; NMDS, nonmetric multidimensional scaling.

dominated by bacteria (termed bacteria-dominant subtype, Bacteria-*T*), and the other subtype was with a microbial community structure dominated by the virus (termed virus-dominant subtype, Virus-*T*).

Two methods, LEfSe and random forest analysis, were conducted to search for differentially enriched microbes between two molecular subtypes. The LEfSe analysis was performed based on the Wilcoxon or Kruskal-Wallis rank sum test and LDA, and the species with statistically significant differences in relative abundance between the two groups were shown by LDA effect size taxonomic cladogram (threshold value with LDA score > 4) (Figure 3B). *E. coli*, *Shigella dysenteriae*, *Babesia bigemina*, and *Pannonibacter phragmitetus*

were prominently detected in Bacteria-*T*, while HBV was prominently detected in Virus-*T*. According to mean decrease accuracy and mean decrease Gini indices, random forest analysis revealed that the top 7 species with the most significant differences in relative abundance between Bacteria-*T* and Virus-*T* were HBV, *E. coli*, *Pannonibacter phragmitetus, Escherichia virus G7C, Babesia bigemina*, *Escherichia virus IME11,* and *Shigella dysenteriae*, with a threshold value of mean decrease accuracy >7.5 and mean decrease Gini >0.6 (Figure 3C).

We further assessed microbial alpha diversity of 2 molecular types, and Chao 1, Shannon, and Simpson analyses revealed that Virus-*T* was with significantly lower community richness and evenness than that of Bacteria-*T* ($p < 0.01$) (Figure 3D). Anosim also showed significant differences in microbial structure differences between the two subtypes ($R = 0.987$ and $p = 0.01$) (Figure 3E).

In addition, we further clarify the association between our IMH-based molecular subtype with typical molecular subclassification of HCC established on the basis of a large cohort.[9] The average expressions of each subtype and each sample were counted after the marker genes and tumor samples were standardized. We found that Bacteria-*T* was more inclined to subclass S1, while Virus-*T* was more inclined to subclass S3 (Figure 3F). As reported, compared with subclass S3, subclass S1 was with larger volume and poorer differentiation, and was associated with a significantly greater risk of earlier recurrence ($p < 0.05$). In addition, subclass S1 exhibited more vascular invasion and satellite lesions (both known risk factors for early recurrence). Consistent with this observation, Bacteria-*T* was also associated with a more invasive phenotype.

For the bacteria-dominant subtype, Anosim analysis ($R = -0.046$, $p = 0.98$) showed a similar microbial structure between tumor tissues (Bacteria-*T*) and the corresponding adjacent tissues (Bacteria-*N*) (Figure 3G), as confirmed by multiresponse permutation procedure based on the Bray-Curtis distance ($p = 0.653$). Meanwhile, Bacteria-*T* and Bacteria-*N* were with similar community richness and evenness as indexed by Chao 1, Shannon, and Simpson indexes ($p > 0.05$) (Figure 3H).

Different microbiome-based molecular subtypes correlated with discrepant clinical-pathologic features of HCC

Clinical and pathologic data of HCC cases were collected and analyzed. Bacteria-T was with larger tumor diameter ($p = 0.041$), more frequent capsular invasion ($p = 0.027$), and higher plasma D-dimer level ($p = 0.047$) compared with Virus-*T* (Figure 3I). No statistical differences were found between the two subtypes at the plasma AFP level, tumor differentiation degree, microvascular invasion, satellite nodule, tumor necrosis, TNM stage, or BCLC stage. We also analyzed the correction between IMH with liver cirrhosis and portal hypertension. Portal hypertension was defined by the presence of esophagogastric varices and/or a platelet count $< 100 \times 10^9$/L in association with splenomegaly,[20] while no statistical differences were found ($p = 1.000$). Furthermore, we analyzed the association between the viral load of HBV in tissue samples and IMH, and the results showed that the viral load of HBV in Virus-*T* was higher than in Bacteria-*T*, while no statistical differences were found ($p = 0.564$). The clinical and pathologic data were shown in Supplemental Table S3 (http://links.lww.com/HEP/H820).

A total of 3 patients recurred during a median 12 months of follow-up after the operation, of which 2 in 8 patients (25%) recurred in Bacteria-*T* and one in 21 patients (4.76%) recurred in Virus-*T*. Disease-free survival of patients in Bacteria-T was shorter than that of Virus-*T* although no statistical difference was found ($p = 0.153$)

Discrepant gene signatures between two subtypes were mainly enriched in immune and metabolism-related pathways

Transcriptome sequencing was performed on 24 samples (12 paired tumor tissues and corresponding adjacent tissues), in which Bacteria-T and Virus-T accounted for half, respectively. A total of 323 DEGs were identified with a threshold of $p < 0.01$ and $|\log2FoldChange| \geq 1$, including 162 upregulated and 161 downregulated genes in Virus-T compared with Bacteria-T. The top 50 DEGs were listed in Supplemental Tables S4 (http://links.lww.com/HEP/H821). The hierarchical cluster analysis indicated discrepant gene signatures between the two subtypes (Figure 4A). The gene ontology enrichment analysis revealed that DEGs between two subtypes were mainly enriched in gene ontology terms related to chemoattractant activity, steroid hydroxylase activity, and LDL particle binding in molecular functions; immunoglobulin complex and protein-lipid complex in cellular component; and immunoglobulin production, production of molecular mediator of immune response, and lymphocyte-mediated immunity in biological processes (Figure 4B), which were mainly immune and metabolism-related pathways.

In addition, a total of 147 DEGs were identified with a threshold of $p_{adj} \leq 0.05$ and $|\log_2FoldChange| \geq 1$, including 118 upregulated and 29 downregulated genes in tumor tissues compared with the corresponding adjacent tissues. The KEGG enrichment analysis revealed that DEGs between tumor tissues and the corresponding adjacent tissues were mainly enriched in cell cycle, p53 signaling pathway, viral protein interaction with cytokine and cytokine receptor, neuroactive ligand–receptor interaction, and cytokine-cytokine receptor interaction.

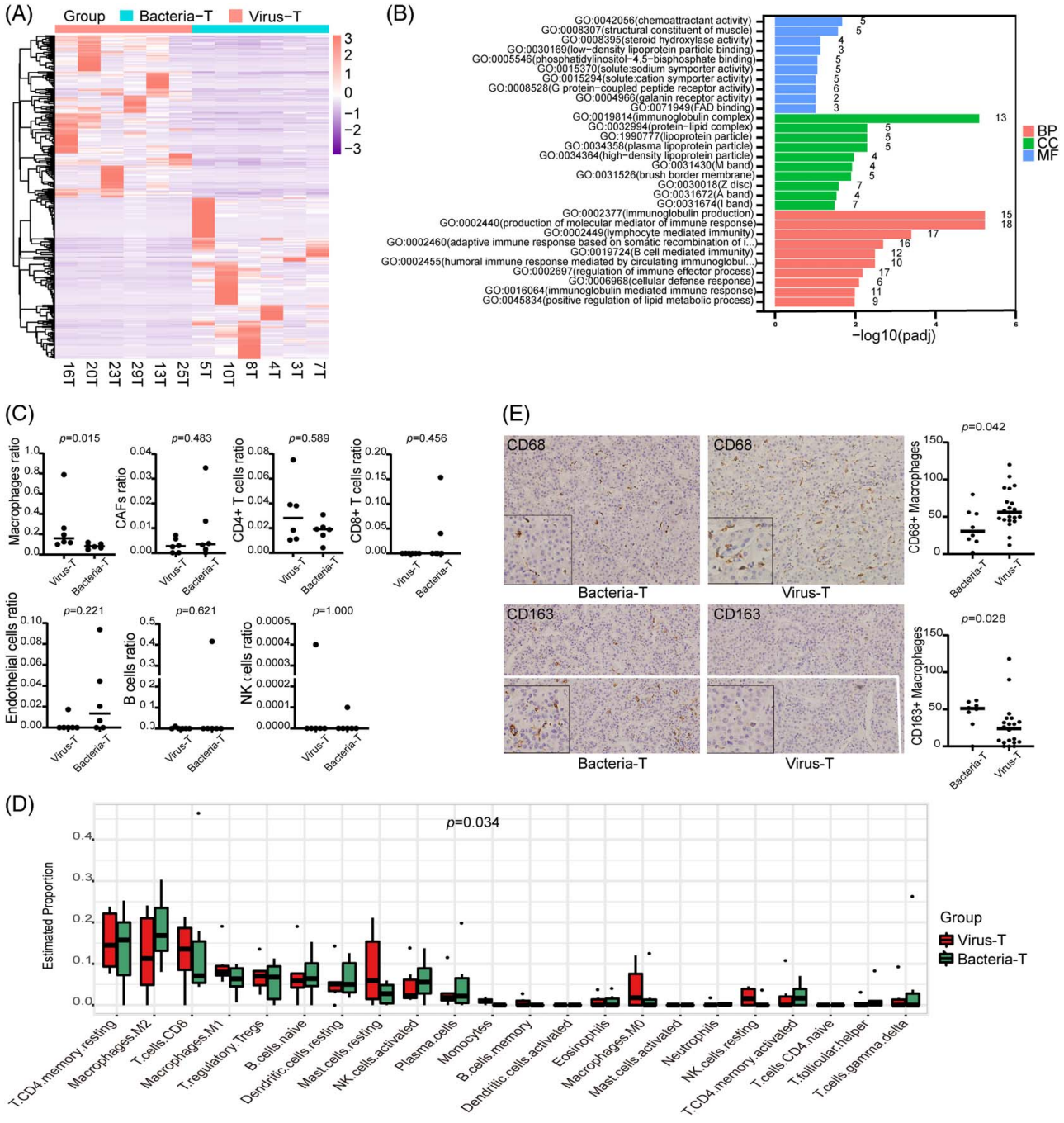

FIGURE 4 Discrepant gene signatures between two HCC molecular subtypes were mainly enriched in immune and metabolism. (A) Two HCC molecular subtypes were with different gene signatures by hierarchical cluster analysis. (B) Top 10 enriched GO terms in BPs, MFs, and CC. (C) Proportions of macrophages, CAFs, $CD4^+$ T cells, $CD8^+$ T cells, B cells, NK cells, and endothelial cells by EPIC. (D) Proportions of 22 immune cell subtypes by CIBERSORT. (E) IHC staining of $CD68^+$ and $CD163^+$ macrophages of two HCC molecular subtypes. Abbreviations: BP, biological process; CAF, cancer-associated fibroblast; CC, cellular component; GO, gene ontology; IHC, immunohistochemistry, MF, molecular function.

Higher infiltration of M2 macrophage was detected in Bacteria-*T* rather than Virus-*T*

To characterize the disparity of tumor immune microenvironment between two molecular subtypes of HCC, RNA-seq data were imported into EPIC to compute immune cell proportion. The relative proportion of macrophages in Bacteria-*T* was lower than that in Virus-*T* ($p = 0.015$), while no significant differences were found in relative proportions of cancer-associated fibroblasts, $CD4^+$ T cells, $CD8^+$ T cells, B cells, NK cells, and endothelial cells ($p > 0.05$) (Figure 4C).

CIBERSORT was further adopted to identify immune cell subtypes based on RNA-seq data. Accordingly, the

relative proportion of monocytes was significantly different between the two subtypes ($p = 0.034$) while with an extremely small amount. For macrophages, Bacteria-*T* was characterized by higher infiltration of M2 macrophage but lower infiltration of M1 macrophage compared with Virus-*T* (Figure 4D).

To verify the mentioned findings, immunohistochemistry staining was further adopted, and we found that Bacteria-*T* was with lower proportion of $CD68^+$ macrophages ($p = 0.042$) but a higher proportion of $CD163^+$ M2 macrophages ($p = 0.028$) compared with Virus-*T* (Figure 4E), while no significant differences were found at the proportions of $CD3^+$ T cells, CD8+ T cells, and PD-L1 ($p > 0.05$).

Multiple metabolism pathways were upregulated in Bacteria-*T* compared with Virus-*T*

To reveal metabolic heterogeneity between the two subtypes, GSVA was used to calculate the enrichment score of multiple metabolic pathways in each HCC sample based on RNA-seq data. Compared with Virus-*T*, amino acid, carbohydrate, energy, glycan, and lipid metabolism were upregulated in Bacteria-*T* (Figure 5A). We further adopted GSVA to reveal the association between metabolic pathways and immune infiltration, and the result showed that macrophage infiltration was positively correlated with amino acid metabolism (Figure 5B), which coincided with the mentioned finding that Bacteria-*T* was characterized by higher infiltration of M2 macrophage. Correlation analysis between the intratumoral microbiome and metabolic pathways showed that different microbiota induced discrepant metabolic changes. *E. coli* mainly induced upregulation of the amino acid metabolism pathway, while HBV mainly induced upregulation of the glycan metabolism pathway, suggesting that IMH might be responsible in part for the shift of HCC metabolism reprogramming (Figure 5B).

A 3-gene risk signature containing *CSAG4*, *PIP4P2*, and *TOMM5* was filtered out between two subtypes to predict clinical prognosis of HCC patients

First, we chose $\beta = 20$ ($R^2 = 0.8$) to construct the scale-free network based on DEGs between two HCC subtypes by weighted gene coexpression network analysis (Supplemental Figure S2A, http://links.lww.com/HEP/H822), and 9 coexpression modules were finally identified (Supplemental Figure S2B, S2C, http://links.lww.com/HEP/H822). Next, module-trial correlation heatmaps were drawn to assess the correlation between gene modules with significant clinical signatures (tumor diameter and capsular invasion), and the brown module was selected as a clinically significant module (Supplemental Figure S2D, http://links.lww.com/HEP/H822). In addition, we evaluated the correlation between gene modules with clinical signatures by calculating gene significance, which was defined as the average gene significance of all genes in the module, and the brown module was also collected as the hub module (Supplemental Figure S2E, http://links.lww.com/HEP/H822). Thirty-three genes with high connectivity in the brown module were identified as hub genes according to the cutoff criteria ($|MM| > 0.7$ and $|GS| > 0.2$), and 3 genes (*CSAG4, PIP4P2,* and *TOMM5*) were filtered out to be correlated with overall survive ($p < 0.05$) by the Cox regression analysis and constructed a gene risk signature for HCC, which was further verified using the Cancer Genome Atlas data to predict clinical prognosis of HCC patients. According to the median risk score, HCC patients were divided into a high-risk group ($n = 184$) and a low-risk group ($n = 184$). The Kaplan-Meier survival curve showed that patients in the high-risk group were with a statistically lower probability of overall survive compared with the low-risk group ($p = 0.0029$) (Supplemental Figure S2F http://links.lww.com/HEP/H822).

DISCUSSION

This is a case-control study that comprehensively characterized the microbial landscape of liver tissues during the evolution from CHB to HCC. It uncovered IMH of HBV-related HCC tissues adopting mNGS, which can not only accurately identify bacteria at the species level but also can detect viruses, parasites, and fungi, resulting in a more accurate molecular typing. Our study creatively established microbiome-based molecular subtyping of HBV-related HCC and demonstrated that IMH of HCC was correlated with the disparity of clinical-pathologic features and TME. Furthermore, we constructed a 3-gene risk signature between the two subtypes, which can be used to predict the clinical prognosis of HCC patients.

Emerging studies indicate that the intratumoral microbiome is a component of the TME. It can induce inflammation and immune response to affect tumorigenesis and development.[21–24] Specific bacteria (mainly *E. coli*) could damage the intestinal vascular barrier, colonize in the liver, and recruit immune cells, such as macrophages, neutrophils, and monocytes, which resulted in the premetastasis microenvironment in colorectal cancer.[25] To a great extent, metabolism plays an important role in the crosstalk between the intratumoral microbiome and the immune microenvironment.[26] A recent study indicated that intestinal flora-mediated bile acid metabolism regulated HCC tumorigenesis through interfering NKT cells and mediated the innovative mechanism of antitumor immunity.[27] This study

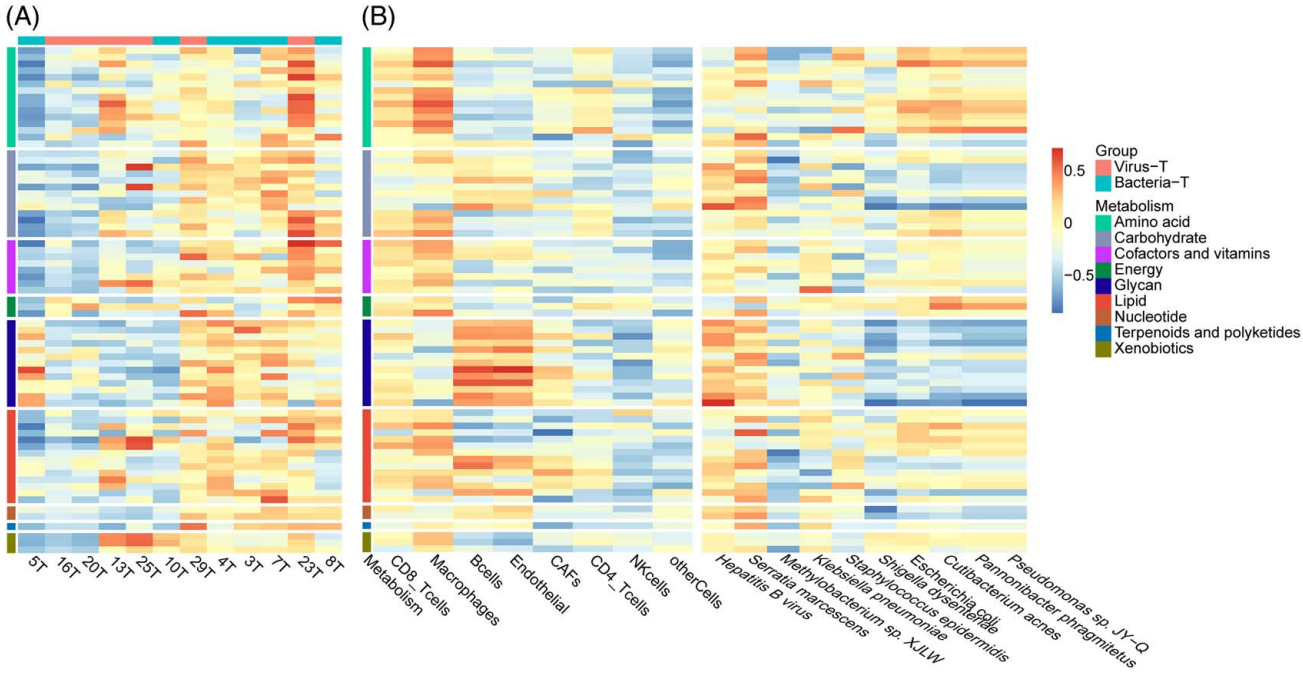

FIGURE 5 Correlation analyses among intratumoral microbiome, immune infiltration, and metabolic features by GSVA. (A) Amino acid, carbohydrate, energy, glycan, and lipid metabolism were upregulated in Bacteria-*T* compared with Virus-*T*. (B) Macrophage infiltration was positively correlated with amino acid metabolism. *Escherichia coli* mainly induced upregulation of the amino acid metabolism pathway. HBV mainly induced upregulation of the glycan metabolism pathway. Abbreviation: GSVA, gene set variation analysis.

provided a new theoretical sight and basis for HCC treatment by regulating bile acid metabolism and intestinal flora. In addition, short-chain fatty acids (intestinal bacterial metabolism products) were reported to reduce liver injury by inhibiting macrophage activation, proinflammatory cytokine production, and neutrophil infiltration through the reduction of lipopolysaccharide translocation.[28] Similarly, we found that Bacteria-*T* was accompanied by more infiltration of M2 macrophage and multiple upregulated metabolism pathways compared with Virus-*T*. This suggested the regulation effect metabolism played between the intratumoral microbiome and the immune microenvironment. Therefore, we inferred that IMH of HCC might affect the immune microenvironment by regulating metabolism reprogramming, which might be responsible for the development and progression of HBV-related HCC and proposed as a potential diagnostic biomarker of HCC. To a certain extent, our IMH-based molecular subtype was overlapped with reported molecular subclassification of HCC. This also indicated its potential for developing effective targeted therapies and evaluating the prognosis.

Another important issue is the origin of the intratumoral microbiome. Although emerging studies estimated the existence of microbiota in tumor tissues,[11,16,17,23,29] its origin was still unclear. Previous studies on pancreatic cancer indicated that the intratumoral microbiome was associated with intestinal dysbiota and translocation.[30,31] Bacteria might migrate into the pancreas from the gut through the pancreatic duct.[32] In our study, the common gut flora, *E. coli* and *Shigella dysenteriae*, were prominently detected, suggesting that retrograde bacterial migration from the gut to the liver might be a source of HCC-related bacteria. In addition, our findings indicated that the microbial community of Bacteria-*T* had a high degree of similarity with the corresponding adjacent tissues. This suggested that the intratumoral microbiome might originate from the adjacent tissue, which was consistent with previous research.[16] This phenomenon might be attributed to the disorganized and permeable vasculature of tumors, as well as the heterogeneous immunosuppressed environment that accelerates the process. Therefore, further intensive studies are required to elucidate the transport processes and underlying mechanisms.

Certainly, there are some limitations to our study. The study was performed on a heterogeneous patient population with a relatively small size. This might affect the generalization of the results. In the next work, a large, random, multicenter prospective clinical trial needs to be carried out to further verify the clinical significance of microbiome-based HCC subtyping and the prognosis-predictive value of the 3-gene risk signature. In addition, our study was limited to HBV-related HCC, and whether it was applicable to HCC caused by other causes remained to be further verified. In conclusion, microbiome-based molecular subtyping

demonstrated IMH of HBV-related HCC was correlated with a disparity in clinical-pathologic features and TME, which might be proposed as a biomarker for prognosis prediction of HBV-related HCC.

AUTHOR CONTRIBUTIONS

Wei Lu and Jinpu Yu: conceived and designed the experiments. Shengnan Li and Zeyu Wang: performed the experiments. Han Xia, Xiehua Zhang, Shu Fan, Qiaoling Zhang, and Yingnan Ye: were responsible for bioinformatics analysis. Shengnan Li and Jinpu Yu: prepared all of the figures and wrote the manuscript. Shengnan Li, Zeyu Wang, Tianqiang Song, Jiayu Lv, Liang Xu, and Qian Li: collected the samples. Han Xia, Ningning Zhang, Jiayu Lv, Hongcheng Lv, and Xiaofen Yue: supported and supervised the research.

FUNDING INFORMATION

This study was supported by the Key Project of Science and Technology, Tianjin Municipal Science and Technology Bureau (19YFZCSY00020).

CONFLICTS OF INTEREST

The authors have no conflicts to report.

ORCID

Shengnan Li https://orcid.org/0000–0002–3458–218X
Han Xia https://orcid.org/0000–0002–5179–0255
Jinpu Yu https://orcid.org/0000–0002–5982–2266
Wei Lu https://orcid.org/0000–0001–7661–9975

REFERENCES

1. Forner A, Reig M, Bruix J. Hepatocellular carcinoma. Lancet. 2018;391:1301–4.
2. Bray F, Ferlay J, Soerjomataram I, Siegel RL, Torre LA, Jemal A. Global cancer statistics 2018: GLOBOCAN estimates of incidence and mortality worldwide for 36 cancers in 185 countries. CA Cancer J Clin. 2018;68:394–424.
3. Yang JD, Hainaut P, Gores GJ, Amadou A, Plymoth A, Roberts LR. A global view of hepatocellular carcinoma: trends, risk, prevention and management. Nat Rev Gastroenterol Hepatol. 2019;16:589–604.
4. Villanueva A. Hepatocellular carcinoma. N Engl J Med. 2019; 380:1450–62.
5. Lee JW, Stone ML, Porrett PM, Thomas SK, Komar CA, Li JH, et al. Hepatocytes direct the formation of a pro-metastatic niche in the liver. Nature. 2019;567:249–52.
6. Lawal G, Xiao Y, Rahnemai-Azar AA, Tsilimigras DI, Kuang M, Bakopoulos A, et al. The immunology of hepatocellular carcinoma. Vaccines (Basel). 2021;9:1184.
7. Ringelhan M, Pfister D, O'Connor T, Pikarsky E, Heikenwalder M. The immunology of hepatocellular carcinoma. Nat Immunol. 2018;19: 222–32.
8. Boyault S, Rickman DS, de Reyniès A, Balabaud C, Rebouissou S, Jeannot E, et al. Transcriptome classification of HCC is related to gene alterations and to new therapeutic targets. Hepatology. 2007;45:42–52.
9. Hoshida Y, Nijman SMB, Kobayashi M, Chan JA, Brunet JP, Chiang DY, et al. Integrative transcriptome analysis reveals common molecular subclasses of human hepatocellular carcinoma. Cancer Res. 2009;69:7385–92.
10. Garrett WS. Cancer and the microbiota. Science. 2015;348:80–6.
11. Riquelme E, Zhang Y, Zhang L, Montiel M, Zoltan M, Dong W, et al. Tumor microbiome diversity and composition influence pancreatic cancer outcomes. Cell. 2019;178:795–806 e12.
12. Sia D, Jiao Y, Martinez-Quetglas I, Kuchuk O, Villacorta-Martin C, Castro de Moura M, et al. Identification of an immune-specific class of hepatocellular carcinoma, based on molecular features. Gastroenterology. 2017;153:812–26.
13. Gao Q, Zhu H, Dong L, Shi W, Chen R, Song Z, et al. Integrated proteogenomic characterization of HBV-related hepatocellular carcinoma. Cell. 2019;179:1240. doi:10.1016/j.cell.2019.10.038
14. Bruix J, Gores GJ, Mazzaferro V. Hepatocellular carcinoma: clinical frontiers and perspectives. Gut. 2014;63:844–55.
15. Nault JC, Martin Y, Caruso S, Hirsch TZ, Bayard Q, Calderaro J, et al. Clinical impact of genomic diversity from early to advanced hepatocellular carcinoma. Hepatology. 2020;71:164–82.
16. Nejman D, Livyatan I, Fuks G, Gavert N, Zwang Y, Geller LT, et al. The human tumor microbiome is composed of tumor type-specific intracellular bacteria. Science. 2020;368:973–80.
17. Yachida S, Mizutani S, Shiroma H, Shiba S, Nakajima T, Sakamoto T, et al. Metagenomic and metabolomic analyses reveal distinct stage-specific phenotypes of the gut microbiota in colorectal cancer. Nat Med. 2019;25:968–76.
18. Guo W, Zhang Y, Guo S, Mei Z, Liao H, Dong H, et al. Tumor microbiome contributes to an aggressive phenotype in the basal-like subtype of pancreatic cancer. Commun Biol. 2021;4:1019.
19. Xiao P, Long X, Zhang L, Ye Y, Guo J, Liu P, et al. Neurotensin/IL-8 pathway orchestrates local inflammatory response and tumor invasion by inducing M2 polarization of Tumor-Associated macrophages and epithelial-mesenchymal transition of hepatocellular carcinoma cells. Oncoimmunology. 2018;7:e1440166.
20. Zhong J, Ke Y, Gong W, Xiang B, Ma L, Ye X, et al. Hepatic resection associated with good survival for selected patients with intermediate and advanced-stage hepatocellular carcinoma. Ann Surg. 2014;260:329–40.
21. Baruch EN, Wang J, Wargo JA. Gut microbiota and antitumor immunity: Potential mechanisms for clinical effect. Cancer Immunol Res. 2021;9:365–70.
22. Fessler J, Matson V, Gajewski TF. Exploring the emerging role of the microbiome in cancer immunotherapy. J Immunother Cancer. 2019;7:108.
23. Sepich-Poore GD, Zitvogel L, Straussman R, Hasty J, Wargo JA, Knight R. The microbiome and human cancer. Science. 2021; 371:6536.
24. Sethi V, Vitiello GA, Saxena D, Miller G, Dudeja V. The role of the microbiome in immunologic development and its implication for pancreatic cancer immunotherapy. Gastroenterology. 2019; 156:2097–115 e2.
25. Bertocchi A, Carloni S, Ravenda PS, Bertalot G, Spadoni I, Lo Cascio A, et al. Gut vascular barrier impairment leads to intestinal bacteria dissemination and colorectal cancer metastasis to liver. Cancer Cell. 2021;39:708–24 e11.
26. Bidkhori G, Benfeitas R, Klevstig M, Zhang C, Nielsen J, Uhlen M, et al. Metabolic network-based stratification of hepatocellular carcinoma reveals three distinct tumor subtypes. Proc Natl Acad Sci U S A. 2018;115:E11874–83.
27. Ma C, Han M, Heinrich B, Fu Q, Zhang Q, Sandhu M, et al. Gut microbiome-mediated bile acid metabolism regulates liver cancer via NKT cells. Science. 2018;360:eaan5931.
28. Wang HB, Wang PY, Wang X, Wan YL, Liu YC. Butyrate enhances intestinal epithelial barrier function via up-regulation of tight junction protein Claudin-1 transcription. Dig Dis Sci. 2012;57:3126–5.
29. Wong-Rolle A, Wei HK, Zhao C, Jin C. Unexpected guests in the tumor microenvironment: microbiome in cancer. Protein Cell. 2021;12:426–35.

30. Pushalkar S, Hundeyin M, Daley D, Zambirinis CP, Kurz E, Mishra A, et al. The pancreatic cancer microbiome promotes oncogenesis by induction of innate and adaptive immune suppression. Cancer Discov. 2018;8: 403–16.
31. Frost F, Weiss FU, Sendler M, Kacprowski T, Rühlemann M, Bang C, et al. The gut microbiome in patients with chronic pancreatitis is characterized by significant dysbiosis and overgrowth by opportunistic pathogens. Clin Transl Gastroenterol. 2020;11:e00232.
32. Geller LT, Barzily-Rokni M, Danino T, Jonas OH, Shental N, Nejman D, et al. Potential role of intratumor bacteria in mediating tumor resistance to the chemotherapeutic drug gemcitabine. Science. 2017;357:1156–60.

How to cite this article: Li S, Xia H, Wang Z, Zhang X, Song T, Li J, et al. Intratumoral microbial heterogeneity affected tumor immune microenvironment and determined clinical outcome of HBV-related HCC. Hepatology. 2023;78:1079–1091. https://doi.org/10.1097/HEP.0000000000000427